Satellite-Based Insights into Precipitation Formation Processes in Continental and Maritime Convective Clouds at Nighttime

ITAMAR M. LENSKY AND DANIEL ROSENFELD

Institute of Earth Science, Hebrew University of Jerusalem, Jerusalem, Israel

(Manuscript received 17 May 2002, in final form 26 March 2003)

ABSTRACT

Nighttime microphysical retrievals can be obtained to a much lesser accuracy than those of the daytime, because of lack of the solar radiation. However, a proper treatment of the brightness temperature difference (BTD) between a thermal IR channel (11 μm) and a mid-IR channel (3.7 μm) reveals information about the microstructure and precipitation potential of clouds at nighttime. The two factors that contribute to large BTD are the particle size at cloud top and the optical depth of the cloud layer. These two factors have contradictory effects on precipitation. The respective contributions were simulated and compared with observations of the Tropical Rainfall Measuring Mission. Based on that, a method was developed to use the distribution of BTD with cloud-top temperature for retrieving cloud microstructure and precipitation properties.

1. Introduction

Rosenfeld and Lensky (1998) presented a method to infer the precipitation formation processes in maritime and continental convective clouds at daytime. The method was based on the retrieval of the cloud particle's effective radius near cloud tops, which is done by using the reflected sunlight at a mid-IR channel. This method was later used to show local and large-scale impacts of aerosol on precipitation in Lensky et al. (2000), Rosenfeld (1999, 2000), Rosenfeld et al. (2001), and more. These studies showed that precipitation processes were more efficient in maritime clouds than in continental clouds. Khain et al. (2001) and Reisin et al. (1996) arrived to the same conclusions by doing simulations with cloud models. In this paper, we present new insights into the precipitation formation processes in maritime and continental convective clouds at nighttime and how to use them for detection of cloud microstructure and precipitation potential. In this paper, we use the terms ''maritime'' and ''continental'' clouds in their microphysical sense and not necessarily in their geographical sense.

The conditions for development of precipitation in clouds are 1) sufficient water (thick cloud) and 2) an effective mechanism of converting the small cloud droplets suspended in the air into large precipitation particles.

Precipitation forms when the particles become large enough to have terminal fall velocity of few meters per second, so that they can get to the ground before evaporating. Effective mechanisms of converting cloud water into precipitation are coalescence of cloud droplets (warm processes) and ice aggregation (cold processes). Thick clouds with large particles are likely to have enough column-integrated water and effective coalescence to develop precipitation. Albrecht (1989), Rosenfeld and Gutman (1994), and Lensky and Rosenfeld (1997) used an effective radius of 14–15 μm as a threshold for precipitation for both cold and warm processes in the daytime. We demonstrate in this paper how the brightness temperature (BT) difference (BTD) between a thermal IR channel (11 μm) and a mid-IR channel (3.7 μm) is used at nighttime whereas the reflected sunlight in the mid-IR is used in the daytime.

The next section examines some radiation considerations. A radiative transfer model is used in section 3 to demonstrate the effect of particle size and cloud depth on the BTD. The implementation of the radiation considerations is given in section 4. Case studies for maritime and continental clouds are given in section 5. Summary and conclusions are presented in section 6.

2. Radiation considerations

Inoue (1987) used the BTD between two thermal channels (11 and 12 μm) as a measure for the deviation from a classical blackbody (BB) behavior, where a smaller BTD (closer to classical BB) is typical for thicker clouds. At nighttime, the BTD between a thermal IR channel (11 μm) and a mid-IR channel (3.7 μm) is used to check passing criteria that indicate that cloud depth and particle size are large enough to be considered as precipitating clouds.

If we use the subscript i to denote the channel, the

Corresponding author address: Itamar M. Lensky, Institute of Earth Science, Hebrew University of Jerusalem, Jerusalem 91904, Israel.
E-mail: itamarl@shum.huji.ac.il

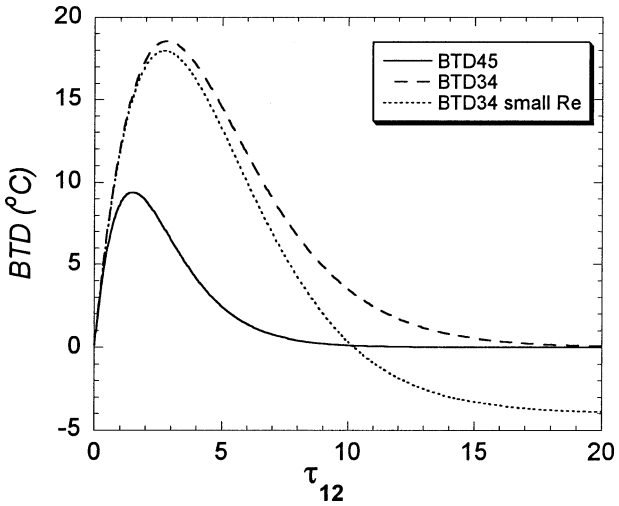

FIG. 1. BTD as a function of optical depth (τ_{12}). Cloud-top temperature is 250 K, and ground temperature is 300 K. The thick line is for T_{11-12}, the dashed line is for $T_{3.7-11}$, and the dotted line is the same as $T_{3.7-11}$ but for clouds with small particles.

emissivity of clouds ε_i can be expressed in terms of optical depth τ_i:

$$\varepsilon_i = a_i(1 - e^{-\tau_i}), \tag{1}$$

where a_i stands for the effect of scattering on the emissivity.

The single scattering albedo of cloud droplets at 11 or 12 μm is nearly zero ($a_{11} = 1$), but scattering is not negligible at 3.7 μm ($a_{3.7} < 1$) and depends on the particle size distribution. At nighttime, the scattering by cloud droplets reduces the cloud emissivity and shields some of the warmer radiation from the ground or lower portions of the cloud itself. Rosenfeld et al. (2003) showed that the cloud optical depth with a given water content is greater by a factor of about 6 for clouds with small (i.e., $r_e = 5$ μm) as compared with large (i.e., $r_e = 30$ μm) droplets, where r_e is effective radius.

The outgoing radiance R_i for a completely cloud-covered scene will take the form

$$R_i = \varepsilon_i B_i(T_c) + (1 - \varepsilon_i)B_{gi}, \tag{2}$$

where $B_i(T_c)$ is the Plank function at cloud-top temperature T_c and $B_{gi}$is the cloud-free upwelling radiance from the ground.

If we neglect atmospheric contribution, the BTD T_{ij} between channels i and j will be

$$T_{ij} = B_i^{-1}(R_i) - B_j^{-1}(R_j), \tag{3}$$

where $B_i^{-1}(R_i)$ is the inverse Plank function in kelvins.

Wu (1987) made some sensitivity studies using detailed radiative transfer model and found large variations of BTD between the 11- and 12-μm channels (T_{11-12}) when assuming different particle size distributions (Fig. 6 in Wu 1987). In general, smaller T_{11-12} was found for clouds with larger particles.

Figure 1 shows a plot of the BTD as function of the optical depth τ_i for a cloud with top temperature T_c of 250 K and ground temperature of 300 K. The thick line is for T_{11-12}, the thin line is for $T_{3.7-11}$, and the broken line is the same as $T_{3.7-11}$ but for clouds with small particles that reduce the 3.7-μm emissivity and the 3.7-μm brightness temperature. For the clouds with small particles, we decreased T_c in Eq. (2) by 4 K to match observations and results of radiative transfer model calculations that will follow in section 3. Figure 1 shows that for small optical depth in the 12-μm channel (τ_{12}) all of the BTD curves increase with increasing τ_{12} up to a maximum at τ_{12} of about 2. We are interested in the precipitating clouds. Thin clouds ($\tau_{12} < 3$) do not precipitate; therefore, we will concentrate on clouds with larger optical depth. In the range of $\tau_{12} > 8$, there is no additional information from the T_{11-12} curve on cloud depth. Nevertheless, even for τ_{12} 2 times as large, the $T_{3.7-11}$ curve varies with cloud depth and, even more, according to the microphysics of the cloud top: negative $T_{3.7-11}$ values for small particles near cloud top and (small) positive or zero values for large particles near cloud top. The negative $T_{3.7-11}$ is a result of the effective scattering of small particles at 3.7 μm, which decreases the brightness temperature at 3.7 μm. In contrast, the same cloud would behave as blackbody at 11 or 12 μm if it were optically thick enough because of the low scattering efficiency, resulting in negative $T_{3.7-11}$ for optically thick clouds.

3. Radiative transfer model

A more comprehensive understanding of the T_{11-12} and $T_{3.7-11}$ behavior can be gained by using a detailed radiative transfer (RT) code. The Santa Barbara discrete ordinate radiative transfer (DISORT) atmospheric RT (SBDART) was used for nighttime (no solar radiation), with atmospheric profile type 2 (midlatitude summer 2.9 g vapor cm^2), aerosol model 1 (rural), albedo model 6 (vegetation), cloud-layer altitudes of 4 km (cloud-top temperature at 260 K), and an observation altitude at 100 km. A description of SBDART can be found in Ricchiazzi et al. (1998), and the application was available online at http://arm.mrcsb.com/sbdart.

The results of 31 runs of the RT model for a cloud with top temperature of 260 K, different optical thickness at 0.55 μm (τ from 0.01 to 100), and effective radius of 5–35 μm and one run for clear sky are presented in Fig. 2. Figure 2a shows the T_{11-12} and $T_{3.7-11}$ that correspond to cloud of optical depth and effective radius as indicated in Fig. 2b. In the right-hand side of Fig. 2a there is one calculation for clear sky (ground temperature 290 K), with BTD resulting only from atmospheric effects, followed by a cloud layer with small droplets (5 μm) that becomes optically thicker (from 0.01 to 100) as one moves leftward. As one goes farther to the left, the effective radius increases in a cloud of constant optical depth of 100, until $r_e = 35$ μm. On the left-hand side of Fig. 2a, the cloud optical depth de-

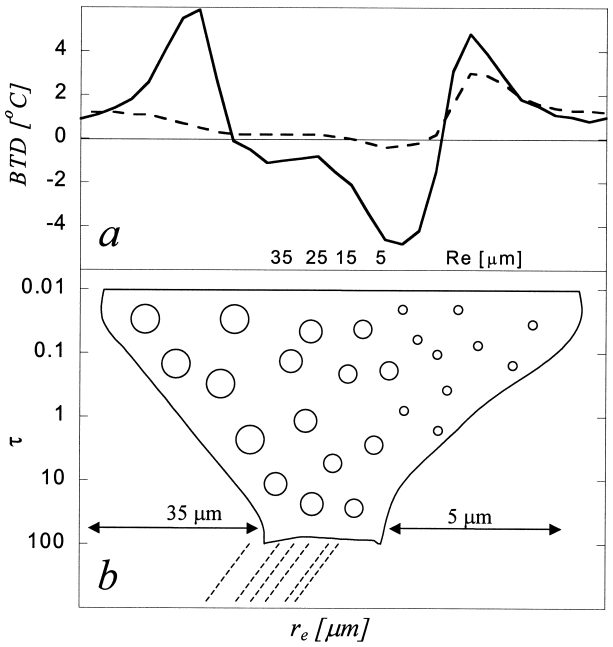

FIG. 2. (a) The BTD for clouds with varying particle effective radii r_e and optical thickness $\tau_{0.55}$ calculated by the RT model. (b) The input to the RT model is schematically represented, where the cloud droplet's effective radii vary along the horizontal axis and the optical thickness of the cloud varies along the vertical axis.

creases down to 0.01, with large particles, and finally decreases to zero (clear sky).

The $T_{3.7-11}$ curve in both sides of the hypothetical cloud (i.e., shallow cloud layer with small and large particles) is nearly symmetric, with a strong influence of the ground for the lower optical depth ($\tau < 0.1$). As the cloud optical depth increases, part of the upwelling radiation interacts with the cloud layer, resulting in a decrease of the indicated cloud-top temperature and an increase of the BTD. The BTD reaches a peak when the cloud is semitransparent ($\tau \sim 2$), and the difference in the emissivity between 3.7 and 11 μm becomes the largest. When the cloud becomes thicker ($\tau > 10$), the effect of the cloud particle size becomes dominant. The 3.7-μm emissivity is much smaller for small particles than for large particles, resulting in a BTD of -4 K for $r_e = 5$ μm.

The effect of particle size on the BTD for thicker clouds ($\tau > 10$) can be seen also for the T_{11-12} curve, but it is too small to be useful. For the thinner clouds ($\tau < 10$), there is an asymmetry in the T_{11-12} curve, where in, on the right-hand side of the T_{11-12} curve, the BTD of the smaller particles ($r_e = 5$ μm) is much larger than that of the larger particles ($r_e = 35$ μm) in the left-hand side of Fig. 2a. This result is in agreement with Fig. 6 in Wu (1987).

4. Implementation of the radiation considerations

Figure 3a presents a more realistic way to look at Fig. 2b. The small particles on the right-hand side of Fig. 2b are presented in Fig. 3a as undeveloped small clouds. Particles with varying sizes at the center of Fig. 2b are presented in Fig. 3a as clouds with precipitating formation processes in different stages. Last, large particles on the left-hand side of Fig. 2b are presented in Fig. 3a as high-level cloud anvils with mainly large ice particles. Two schematic $T_{3.7-11}$ curves are presented as a function of the T_{11} temperature in Fig. 3b: one for maritime clouds and one for continental clouds. The size of water particles of maritime clouds is larger then those of continental clouds. Therefore, $T_{3.7-11}$ is larger for the maritime clouds than for the continental clouds. We can further divide the contributions of the effective radius and optical depth to $T_{3.7-11}$. Figure 3c shows the contribution of optical depth to $T_{3.7-11}$ when the effective radius is kept constant and the contribution of the particle size to $T_{3.7-11}$ when the optical depth is kept constant. The effects of the particle size and optical depth on $T_{3.7-11}$ are summarized qualitatively in Table 1.

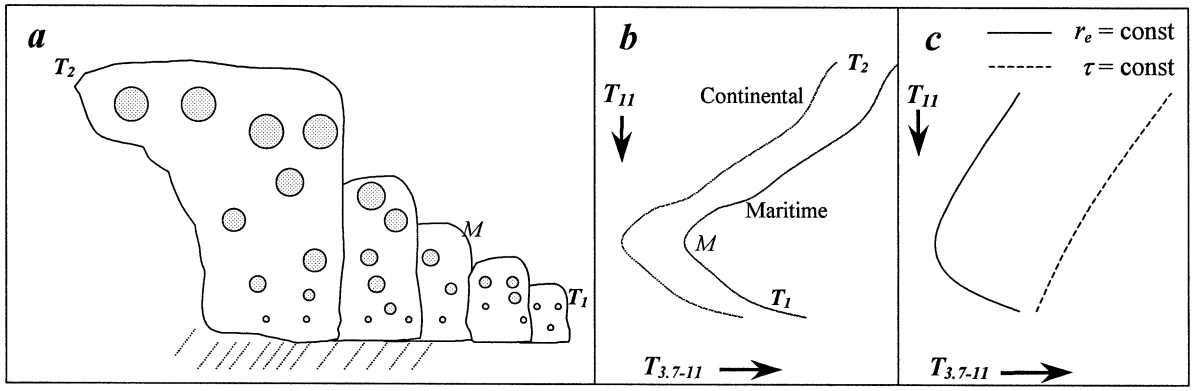

FIG. 3. (a) A more realistic way to look at Fig. 2b. (b) The $T_{3.7-11}$ curve of Fig. 2a is presented schematically as function of the T_{11} temperature. The two $T_{3.7-11}$ curves represent maritime clouds with larger particle sizes and larger $T_{3.7-11}$ than those of continental clouds. (c) The effect of the optical depth and particle size on $T_{3.7-11}$.

TABLE 1. The effects of the effective radius and optical depth on $T_{3.7-11}$.

	Large τ	Small τ
Large r_e	Medium $T_{3.7-11}$	Largest $T_{3.7-11}$
Small r_e	Negative $T_{3.7-11}$	Medium $T_{3.7-11}$

a. The data

The data for this study were obtained from two different instruments on the Tropical Rainfall Measuring Mission (TRMM) satellite. Date from the visible and infrared spectrometer (VIRS) were used for the study, and direct measurements by the precipitation radar (PR) were used for validation.

VIRS is a radiometer with five channels in the visible and infrared wavelengths: 0.65, 1.6, 3.7, 11, and 12 μm. The radiance from the five channels is given in watts per meter. During nighttime, BT is calculated for channels 3, 4, and 5. The operational rain algorithm of the PR was used for validation of the infrared rain formation processes from VIRS.

A total of 236 coincidence subsets of TRMM nighttime passes obtained during 1998 were used for this study. Of these, 133 were obtained from the western Pacific at Kwajalein (9°N, 167°E) and 103 were from the east Mediterranean Sea and Israel (31°N, 35°E). A total of over 5 000 000 cloudy pixels were collected, in both locations. All of the pixels used for this study were in the PR's range.

b. The BTD curves

Figure 4 shows the distribution of all the data on four $T_{3.7-11}$–T_{11} diagrams. On the ordinate are plotted percentiles of pixels with the same cloud-top temperature. For a given cloudtop temperature (T_{11}), the $T_{3.7-11}$ curves denote the percentile of the pixels to the left of the curve. Data that were collected over Israel are plotted in Figs. 4a and 4b, and data that were collected over Kwajalein are plotted in Figs. 4c and 4d. Figures 4a and 4c show precipitating pixels, and Figs. 4b and 4d show nonprecipitating pixels, according to the PR.

In the maritime clouds over Kwajalein, all clouds

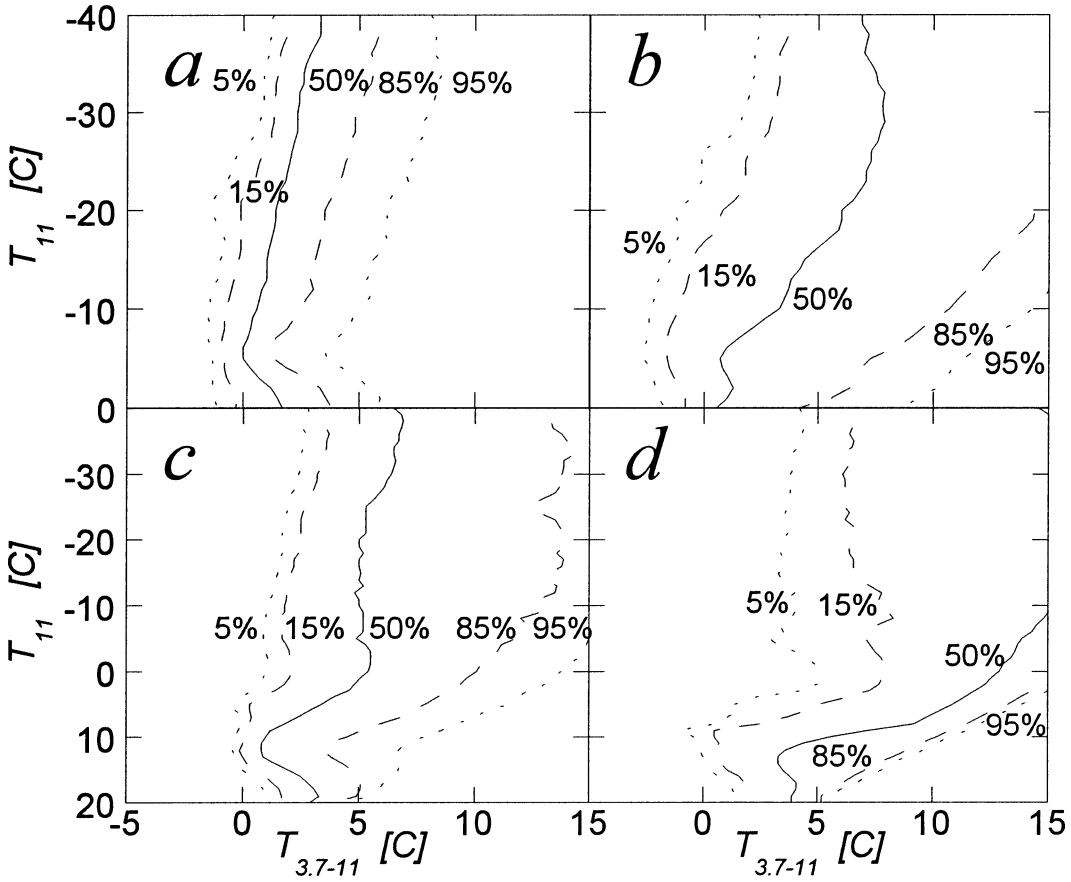

FIG. 4. The $T_{3.7-11}$ curves as a function of the T_{11} temperature over (a), (b) Israel and (c), (d) Kwajalein; (a) and (c) are for precipitating pixels and (b) and (d) are for nonprecipitating pixels, according to the PR. The percentile indicated stands for the percent of (raining or nontraining) pixels to the left of the indicated line. For example, about 50% of the pixels with $T_{11} < -10$°C in (c) have $T_{3.7-11} < 5$°C, and in (d) only about 15% of the pixels with $T_{11} < -10$°C have $T_{3.7-11} < 5$°C.

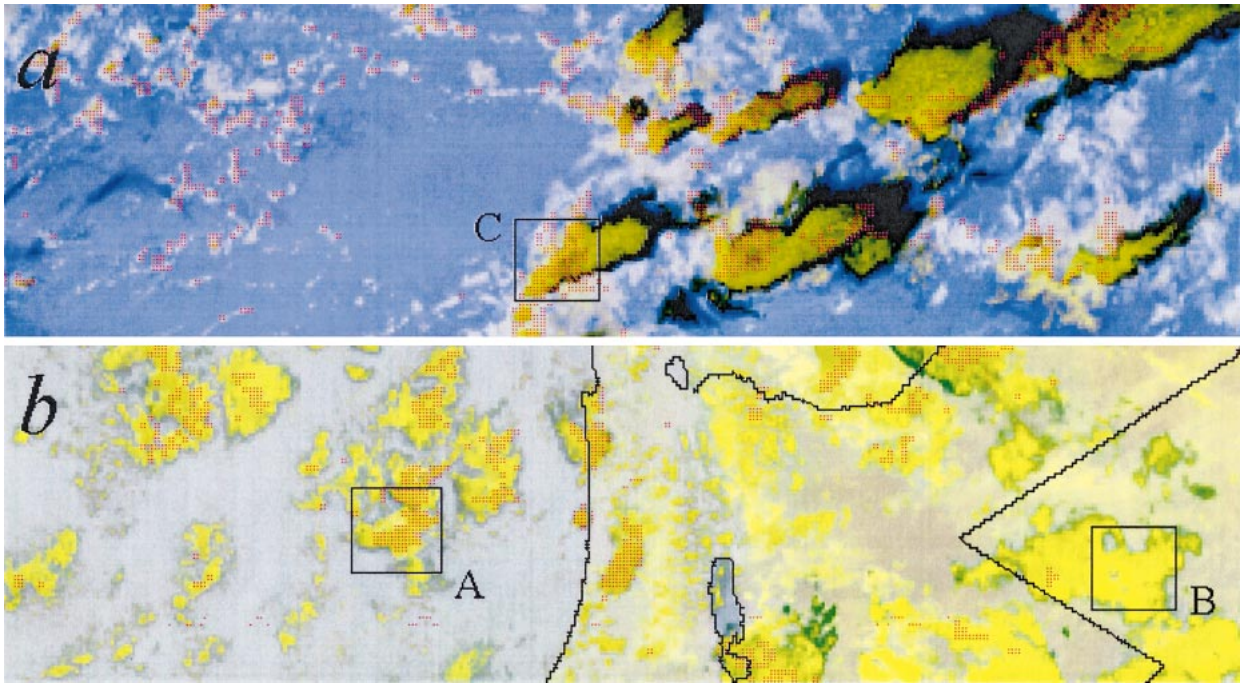

FIG. 5. (a) TRMM image from 1704 UTC 28 Jul 1998 over Kwajalein. (b) TRMM image from 2015 UTC 28 Jan 1998 over the east Mediterranean Sea (A), Israel, and Jordan (B). The red hatching marks the areas in which the TRMM radar detected precipitation. The RGB composition is the following: inverse $T_{3.7-12}$ (red), inverse $T_{3.7-11}$ (green), and T_{11} (blue). Black clouds have high $T_{3.7-12}$ and $T_{3.7-11}$ and low T_{11}; these are cirrus clouds. Yellow–brown clouds have low $T_{3.7-12}$, $T_{3.7-11}$, and T_{11}; these clouds are more likely to rain. The brighter clouds have low $T_{3.7-12}$ and $T_{3.7-11}$ and high T_{11}; these are warm clouds with small particles. The $T_{3.7-11}$ curves of boxes A, B, and C are analyzed in Fig. 6.

have very large particles, even the youngest and nonprecipitating clouds. Only the optical thickness varies between precipitating and nonprecipitating clouds. In continental clouds, the particle size is smaller than that of maritime clouds, with the smallest particle size for the nonprecipitating clouds.

Following Table 1, we will look now in Fig. 4 for the largest (item 1, below) and smallest (item 2, below) $T_{3.7-11}$ and then will compare maritime versus continental clouds (item 3, below) and precipitating versus nonprecipitating clouds (item 4, below). As mentioned above, Fig. 4 represents the whole dataset; a closer look into two case studies will follow in the next section.

1) The two contributions to large $T_{3.7-11}$ are large particles and thin clouds. Figure 4d is of nonprecipitating maritime clouds. These clouds both have large particles and are optically thinner; therefore, these clouds have the largest $T_{3.7-11}$: about 85% of the clouds have $T_{3.7-11} > 7$°C at $T_{11} < 0$°C.
2) The smallest $T_{3.7-11}$ (−2.5°C) can be found in the lower parts ($T > -20$°C) of the fifth-percentile curve of Fig. 4b. These are nonprecipitating continental clouds with the smallest particle size. In the upper parts ($T < -20$°C), this effect is masked by the large $T_{3.7-11}$ of the optically thin nonprecipitating anvils.
3) The $T_{3.7-11}$ of the precipitating maritime clouds (Fig. 4c) is larger than that of the precipitating continental clouds (Fig. 4a), and the $T_{3.7-11}$ of the nonprecipitating maritime clouds (Fig. 4d) is larger than that of the nonprecipitating continental clouds (Fig. 4b). This result is due to the larger particles in the maritime clouds versus continental clouds.
4) Maritime clouds over Kwajalein have very large particles; therefore, optically thinner nonprecipitating clouds of Fig. 4d have larger $T_{3.7-11}$ than the optically thicker precipitating clouds of Fig. 4c. The same trend can be seen where the $T_{3.7-11}$ of nonprecipitating continental clouds in Fig. 4b is larger than those of precipitating continental clouds in Fig. 4a.

5. Case studies

Figure 5a shows clouds forming in pristine air over Kwajalein. The cloud particles' effective radius is typically very large in these clouds, forming rain through warm rain precipitation processes. These are extreme maritime clouds. Continental clouds forming over the Mediterranean Sea, Israel, and Jordan can be seen in Fig. 5b. The cloud particles' effective radius of these clouds is typically much smaller than that of extreme maritime clouds. The red–green–blue (RGB) composition chosen for Fig. 5 is the following: inverse $T_{3.7-12}$ in red, inverse $T_{3.7-11}$ in green, and T_{11} in blue. The sea surface temperature in Kwajalein is warmer by 5°C than

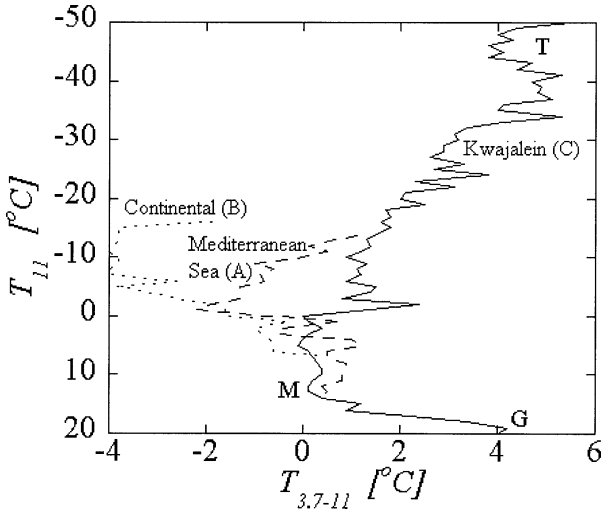

FIG. 6. Fifth-percentile $T_{3.7-11}$ curves as function of the T_{11} temperature of clouds from Fig. 5 over the east Mediterranean Sea (A), Jordan (B), and Kwajalein (C).

in the Mediterranean Sea; therefore, the hue of the sea in Fig. 5a is darker than in Fig. 5b, and the clouds are more ''yellow.'' Black clouds have high $T_{3.7-12}$ and $T_{3.7-11}$ and low T_{11}; these are cirrus clouds. Yellow clouds have low $T_{3.7-12}$, $T_{3.7-11}$, and T_{11}. Brighter clouds in Fig. 5b have low $T_{3.7-12}$ and $T_{3.7-11}$ and high T_{11}; these are warm clouds with small particles. Yellow–brown clouds have middle $T_{3.7-12}$ and $T_{3.7-11}$ values and low T_{11}; these clouds are more likely to rain.

The analysis of the case studies is done on a group of cloudy pixels that were selected in areas ''A,'' ''B,'' and ''C'' of Fig. 5. These areas are of 50 × 50 pixels, small enough so that clouds inside each area can be seen as belonging to one cloud cluster with the same cloud-base temperature and dynamic and thermodynamic parameters. Therefore, smaller drops will be the main reason for lower $T_{3.7-11}$ of clouds with the same cloud-top temperature. Because the cloud drop size grows with time, clouds with smaller particles can be regarded as younger.

The lower fifth-percentile $T_{3.7-11}$ of the clouds in area C of Fig. 5 as function of cloud-top temperature is analyzed in Fig. 6. The signature of the upwelling radiation from the ground through the thin low-level clouds can be seen at point ''G'' with $T_{3.7-11}$ of more than 4 K. As the cloud layer becomes thicker, $T_{3.7-11}$ decreases to a minimum of 0 K at point ''M,'' which is a combination of relatively small particles with sufficiently thick cloud to block the upwelling radiation from the ground. In the interval G–M the cloud is not yet developed enough to produce precipitation. We will be looking for precipitation above the minimum point M. In the case of extreme maritime clouds of Fig. 5a, precipitation is present in curve C of Fig. 6 from point M, that is, clouds colder than +10°C and with $T_{3.7-11} > 0$ until point ''T.'' Pixels with larger particles will be located to the right (larger $T_{3.7-11}$) of the M–T line, but not too far, because thin and broken clouds will produce even larger $T_{3.7-11}$ than that of large particles.

Even the youngest clouds in the extreme maritime environment of Fig. 5a have very large particle radii. Typical precipitating continental clouds, such as those over the Mediterranean Sea, have much smaller effective radii. This can be seen in curve A, where the $T_{3.7-11}$ curves of clouds over the Mediterranean Sea are shifted to smaller $T_{3.7-11}$ with respect to those of Kwajalein (curve C), and even more so for clouds forming over Jordan (curve B). Note the shift of point M to lower T_{11} temperatures and smaller $T_{3.7-11}$ when shifting from curve C to curve A with $T_{11} = -1$°C and $T_{3.7-11} = -2$°C, and then to curve B with $T_{11} = -5$°C and $T_{3.7-11} = -4$°C. The clouds of box A and C precipitate, as can be seen by the PR (the white dots), but those of box B do not precipitate. Therefore, the optical thickness of the clouds of box A is larger than the optical thickness of clouds in box B, and the large $T_{3.7-11}$ of curve A as compared with curve B can be attributed only to the particle size.

The low $T_{3.7-11}$ of curve B is of nonprecipitating clouds; the largest $T_{3.7-11}$ of curve C is due to the ''black'' nonprecipitating anvils. Between these extremes exists a ''$T_{3.7-11}$ precipitation zone.'' This $T_{3.7-11}$ precipitation zone depends on the type of clouds and on T_{11} and is treated in a separate paper (Lensky and Rosenfeld 2003).

6. Summary and conclusions

Dynamic, thermodynamic, and microphysical processes on different scales affect the precipitation. As was shown here, based on simple considerations, radiative transfer model and TRMM satellite observations, the BTD is very sensitive to particle size at cloud top and optical depth of the cloud layer. In the daytime, using the effective radius is relatively simple, because large effective radius indicates that the particle size is large or that the phase of the particles is ice, both contributing to efficient precipitation formation processes. At nighttime, the situation is more complex. Smaller BTD of an optically thick cloud ($\tau_{0.55} > 10$) is related to smaller particle size and, therefore, less efficient precipitation processes. Larger BTD is related to larger particle size or ice cloud and, therefore, more efficient precipitation processes. However, very large BTD is related to semitransparent clouds ($\tau_{0.55} \sim 2$), which are obviously not precipitating. The application of these principles was demonstrated on a large TRMM dataset of precipitating and nonprecipitating clouds according to the PR, in maritime and continental environments. These insights were also applied to two case studies, using a similar approach as reported by Rosenfeld and Lensky (1998), showing clear distinction of cloud microstructure and precipitation potential of clouds in specific areas residing in maritime and continental envi-

ronments. The insights presented in this paper can be readily applied to nighttime delineation of precipitation and investigation of cloud–aerosols interaction.

Acknowledgments. This research has been obtained from the cooperation between the Hebrew University of Jerusalem and NASDA in ADEOS-II Research activity. The research was also funded by the project EURAINSAT, as a shared-cost project cofunded by the Research Directorate General of the European Commission within the research and technological development activities of a generic nature of the Environment and Sustainable Development subprogram (5th Framework Programme).

REFERENCES

Albrecht, B. A., 1989: Aerosols, cloud microphysics and fractional cloudiness. *Science,* **245,** 1227–1230.

Inoue, T., 1987: An instantaneous delineation of convective rainfall areas using split window data of *NOAA-7* AVHRR. *J. Meteor. Soc. Japan,* **65,** 469–481.

Khain, A. P., D. Rosenfeld, and A. Pokrovsky, 2001: Simulating convective clouds with sustained supercooled liquid water down to −37.5°C using a spectral microphysics model. *Geophys. Res. Lett.,* **28,** 3887–3890.

Lensky, M. I., and D. Rosenfeld, 1997: Estimation of precipitation area and rain intensity based on the microphysical properties retrieved from NOAA AVHRR data. *J. Appl. Meteor.,* **36,** 234–242.

——, and ——, 2003: A night-rain delineation algorithm for infrared satellite data based on microphysical considerations. *J. Appl. Meteor.,* **42,** 1218–1226.

——, R. Drori, and D. Rosenfeld, 2000: Large scale view of the effect of aerosol on the onset of precipitation using satellite data. *Proc. 13th Int. Conf. on Clouds and Precipitation,* Reno, NV, ICCP, 314–317.

Reisin, T., S. Tzivion, and Z. Levin, 1996: Seeding convective clouds with ice nuclei or hygroscopic particles: A numerical study using a model with detailed microphysics. *J. Appl. Meteor.,* **35,** 1416–1434.

Ricchiazzi, P., S. Yang, C. Gautier, and D. Sowle, 1998: SBDART: A research and teaching software tool for plane-parallel radiative transfer in the earth's atmosphere. *Bull. Amer. Meteor. Soc.,* **79,** 2101–2114.

Rosenfeld, D., 1999: TRMM observed first direct evidence of smoke from forest fires inhibiting rainfall. *Geophys. Res. Lett.,* **26,** 3105–3108.

——, 2000: Suppression of rain and snow by urban and industrial air pollution. *Science,* **287,** 1793–1796.

——, and G. Gutman, 1994: Retrieving microphysical properties near the tops of potential rain clouds by multispectral analysis of AVHRR data. *J. Atmos. Res.,* **34,** 259–283.

——, and I. M. Lensky, 1998: Satellite-based insights into precipitation formation processes in continental and maritime convective clouds. *Bull. Amer. Meteor. Soc.,* **79,** 2457–2476.

——, Y. Rudich, and R. Lahav, 2001: Desert dust suppressing: A possible desertification feedback loop. *Proc. Natl. Acad. Sci. USA,* **98,** 5975–5980.

——, E. Cattani, S. Melani, and V. Levizzani, 2003: Considerations in daylight operation of 1.6 μm vs 3.7 μm channel on NOAA and Metop satellites. *Proc. 2002 EUMETSAT Meteorological Satellite Conf.,* Dublin, Ireland, EUMETSAT, in press.

Wu, M. C., 1987: A method for remote sensing the emissivity, fractional cloud cover and cloud top temperature of high-level, thin clouds. *J. Climate Appl. Meteor.,* **26,** 225–233.